



Synthesis and characterization of CuZnO@GO nanocomposites and their enhanced antibacterial activity with visible light

Xufei Li¹ · Yangli Che¹ · Yan Lv¹ · Fang Liu¹  · Yongqiang Wang¹ · Chaocheng Zhao¹ · Chunshuang Liu¹

Received: 27 September 2018 / Accepted: 29 October 2018 / Published online: 16 November 2018
© Springer Science+Business Media, LLC, part of Springer Nature 2018, corrected publication 2018

Abstract

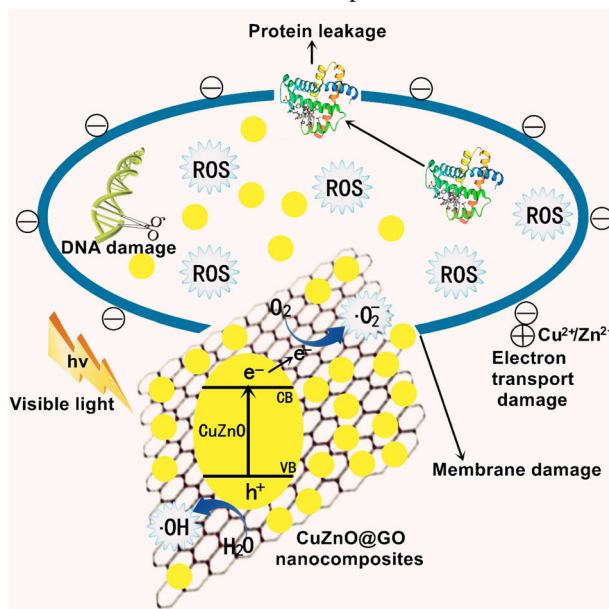
Copper and zinc composite oxide (CuZnO) was synthesized successfully via a sol–gel method and modified by silane coupling agent to prepare CuZnO@graphene oxide (CuZnO@GO) nanocomposites, with CuZnO nanoparticles (NPs) distributed on the GO nanosheets. The structural properties of prepared CuZnO@GO nanocomposites were studied by FT-IR and XRD techniques. SEM and TEM analysis showed the spherical morphology of CuZnO NPs with a diameter of 20–40 nm. The optical properties of synthesized products were estimated through UV–Vis DRS and PL spectroscopy, which suggested that CuZnO@GO nanocomposites had a widened absorption range from UV to visible region and a lower photogenerated carrier recombination rate than that of pure CuZnO NPs. The antibacterial mechanism of CuZnO@GO nanocomposites was investigated using gram-negative bacteria *Escherichia coli* and gram-positive bacteria *Staphylococcus aureus* as two model microorganisms. The antibacterial properties of CuZnO@GO nanocomposites on mixed bacteria were researched in the cooling water system. The results showed that when adding CuZnO@GO nanocomposites to *E. coli* or *S. aureus* suspension, the protein leakage after 20 h was 10.5 times or 8.3 times higher than that in the blank experiment. Furthermore, the antibacterial activity of CuZnO@GO nanocomposites in presence of visible light was found to be significantly enhanced as compared with control. Under visible light irradiation, the antibacterial rate of CuZnO@GO nanocomposites in circulating cooling water reached 99.09% when the mass fraction of GO was 17.5%, and more than 90% of bacteria were inactivated by 100 mg·L⁻¹ CuZnO@GO nanocomposites in 60 min after four recycled runs.

✉ Fang Liu
liufangfw@163.com

¹ Department of Environmental and Safety Engineering, College of Chemical Engineering, China University of Petroleum, Qingdao 266580, China

Graphical Abstract

Schematic of antibacterial mechanism of CuZnO@GO nanocomposites



Highlights

- CuZnO@GO nanocomposites with excellent photocatalytic antibacterial activity were synthesized.
- The antibacterial mechanism of CuZnO@GO nanocomposites was investigated using pure bacteria.
- The antibacterial application of CuZnO@GO nanocomposites for complex bacteria was researched.
- After four recycled runs, the antibacterial rate of CuZnO@GO nanocomposites was still up to 90%.

Keywords CuZnO@GO nanocomposites · Visible light · Photocatalytic antibacterial activity · Antibacterial mechanism · Water treatment

1 Introduction

Along with the development of modernization, water environmental pollution, and water resource shortage have become increasingly prominent. Many factories such as pharmaceutical, chemical, petrochemical, paper, and textile industries have a great demand for water while they also produce large amounts of wastewater which contains various organic compounds, heavy metals, and microorganisms. The growth of microorganisms in wastewater can result in biological slime, pipeline corrosion, and increased water pressure loss [1]. Especially, water contaminated by pathogenic microbes may lead to some waterborne infectious diseases [2]. Therefore, it is of paramount importance to control bacterial growth in wastewater before it is reused or discharged into the environment.

Though conventional chemical disinfection technologies using chlorine, ozone, and chloramines have proven to be highly effective for bacteria inactivation in water treatment, they can react with diverse organic contents in water to form harmful disinfection byproducts, some of which have been identified as mutagenic and carcinogenic [3–5]. Alternative

to these technologies, photocatalytic processes have been widely utilized in recent years due to their efficient, stable and environmentally friendly performance for water decontamination including the degradation of organic pollutants and destruction of bacteria [6]. Typically, efficient photocatalysts such as TiO₂, ZnO, MoS₂, CdS, Ag₃PO₄, etc. have been extensively employed for photocatalytic applications [7–11].

Particularly, zinc oxide (ZnO) chosen for this research is desirable as a suitable material for environmental remediation because of its chemical stability, no toxicity, low cost, a wide band gap (3.37 eV), and a large exciton binding energy (60 meV) [12–14]. The photocatalytic activity of ZnO is comparable and even better than that of TiO₂ in some of reports [15]. Moreover, nanoparticulate ZnO can be used as an antibacterial agent which inhibits both gram-negative bacteria and gram-positive bacteria [16]. However, the photocatalytic antibacterial ability of pure ZnO is valid only under UV light irradiation since the recombination rate of photoinduced electrons and holes of ZnO is too high to effectively make use of visible light. To overcome this limitation, several strategies have been developed to reduce

the recombination of charge carriers by combining the photocatalysts with some noble metals (such as Ag, Pb, and Pt) [17–19] and other semiconductors (like CuO, Fe₂O₃, and CeO₂) [20–22]. Among these materials, copper oxide (CuO) can be used not only to improve the photoactivity of ZnO but also to act as an antibacterial agent itself. Previous studies have revealed that bacteria are not easy to form protective biofilm on the surface of nanoparticulate CuO [23], with the function of inhibiting many kinds of bacteria, which is related to cell membrane damage [24, 25]. In addition to the aforementioned strategies, it has been found that loading of semiconductor photocatalysts on carbon based materials including activated carbon [26], graphene nanosheets [14] or carbon nanotubes [27] holds great promise to enhance the visible light photocatalytic efficiency of photocatalysts.

Graphene and its derivatives have attracted tremendous research efforts in recent years because of their unique structure, large specific surface area and outstanding mechanical, electrical, optical, and thermal performance [28–31]. Furthermore, a lot of research has been done on the antibacterial activity of graphene. In 2010, Hu et al. [32] discovered that graphene had strong antibacterial properties. Okhavan et al. studied the inhibitory of graphene and graphene oxide (GO) nanowalls on *Escherichia coli* and *Staphylococcus aureus* [33]. Compared with graphene, GO exhibits a good hydrophilicity due to more oxygen-containing groups on its surface, and it can be firmly combined with other materials to form complexes through functional groups. It is expected that the combination of ZnO with GO may be ideal to produce superior photocatalytic activity of facilitating the charge separation and transportation due to the conjugated structure and high surface area of GO.

Currently, the research on antibacterial properties of materials is mostly focused on the stage of pure strain, and there are few studies conducted in the complex strain of actual wastewater systems. Hence, in order to ensure that the prepared antibacterial materials can perform in practical applications, it is very necessary to investigate the antibacterial properties of materials in practical wastewater.

Considering the above-mentioned points, in this work, copper and zinc composite oxide (CuZnO) was synthesized via a sol–gel method and modified by silane coupling agent KH550 to combine with GO as the carrier to prepare CuZnO@GO nanocomposites. The synthesized products were characterized by Fourier transform infrared (FT-IR), X-ray diffraction (XRD), scanning electron microscopy (SEM), transmission electron microscope (TEM), ultraviolet–visible diffuse reflectance spectroscopy (UV–Vis DRS) and photoluminescence (PL) spectroscopy techniques. In addition, the antibacterial mechanism of CuZnO@GO nanocomposites was investigated using gram-negative

bacteria *E. coli* and gram-positive bacteria *S. aureus* as two model microorganisms. Finally, the antibacterial properties of CuZnO@GO nanocomposites on mixed bacteria were researched in the cooling water system.

2 Materials and methods

2.1 Preparation of CuZnO NPs and CuZnO@GO nanocomposites

All the reagents in the experiment were of analytical grade purity and were used as received. GO was prepared through a modified Hummers method according to a previous literature [34].

For preparation of CuZnO NPs, 0.035 M of zinc nitrate and 0.015 M of copper acetate were dissolved in 100 mL of ethanol solution (v ethanol:v water = 1:1) by sonication to make mixture uniformly. Then, 0.06 M of citric acid monohydrate was added to the solution. The pH of the solution was adjusted to 5.5–6.7 with aqueous ammonia to obtain dark blue gel. Next, the gel was stirred at 80 °C for 2 h in a water bath to get blue precipitate. After washing with anhydrous ethanol, the blue precipitate was dried at 60 °C and ground to powder. Finally, the powder was calcined at 500 °C for 2 h, and CuZnO NPs were obtained.

For preparation of CuZnO@GO nanocomposites, first of all, the CuZnO NPs obtained above were modified by silane coupling agent KH550 (NH₂CH₂CH₂CH₂Si(OC₂H₅)₃) as a bridge for grafting to promote the combination of CuZnO NPs and GO. Specifically, 0.5 g of CuZnO NPs were dissolved in 10 mL of N-methylpyrrolidone and sonicated for 1 h. Then, 10 mL of silane coupling agent KH550 was added to the solution and sonicated for 2 h to complete the reaction. Afterwards, the precipitate was separated from the solution by centrifugation, washed with anhydrous ethanol, and dried at 60 °C to obtain modified CuZnO NPs. According to a certain mass ratio, GO and modified CuZnO NPs were mixed evenly in dimethylacetamide with ultrasonic treatment for 6 h. Finally, the CuZnO@GO nanocomposites recovered by centrifugation were washed with anhydrous ethanol for three times and dried at 60 °C.

2.2 Characterization

The crystal phase structure of CuZnO@GO nanocomposites was determined by (XRD, X'Pert Pro MPD) manufactured by PANalytical Corporation. The chemical structure of CuZnO@GO nanocomposites was investigated by (FT-IR, NEXUS) spectrometer manufactured by Nicolet Company. The microstructure of CuZnO@GO nanocomposites was analyzed by (SEM, S4800) manufactured by Hitachi Limited and (TEM, JEM-2100UHR) manufactured by Nippon

Electric Corporation. The optical properties of CuZnO@GO nanocomposites were estimated by (UV–Vis DRS), and (PL) spectroscopy.

2.3 Antibacterial mechanism analysis of CuZnO@GO nanocomposites

2.3.1 Protein leakage experiment

The damage of bacterial cell membrane structure will lead to the outflow of cell contents, so the experiment was carried out with the leakage of protein concentration as an indicator [35]. *E. coli* (or *S. aureus*) bacterial suspension with concentration of 10^7 cfu·mL⁻¹ was incubated with CuZnO@GO nanocomposites in conical flasks. In the blank control test, CuZnO@GO nanocomposites were not added to conical flasks. A 1 mL of bacterial suspension was removed into EP tube every 2 h and 5 mL of Coomassie brilliant blue solution was added into the tube. Then the mixture was shaken and reacted for 2 min. The absorbance of the mixed solution was determined at 595 nm and protein concentration was calculated based on the standard curve.

2.3.2 Photocatalytic antibacterial test

The photocatalytic antibacterial activity of CuZnO@GO nanocomposites was evaluated by the inactivation of *E. coli* and *S. aureus* under visible light irradiation. In a typical procedure, 10 mg CuZnO@GO nanocomposites were dispersed into 100 mL of bacterial suspension with concentration of 10^7 cfu·mL⁻¹. Then the mixture solution was exposed to a 300 W Xe lamp with a cutoff filter (providing visible light of $\lambda \geq 420$ nm) under the condition of magnetic stirring. At a given interval of reaction time, 200 μ L of bacterial suspension was taken out and diluted appropriately with sterile distilled water. Subsequently, the dilutions were spread on lysogeny broth (LB) agar plates uniformly and incubated overnight at 37 °C to count the colonies and calculate the number of surviving bacteria. For comparison, the control test without CuZnO@GO nanocomposites was conducted under same visible light irradiation.

2.3.3 Determination of intracellular reactive oxygen species

The level of intracellular reactive oxygen species (ROS) in bacteria was determined by the nitro blue tetrazolium (NBT) reduction method [36]. Bacterial suspensions with

concentration of 10^7 cfu·mL⁻¹ were cultured at 37 °C for 5, 10, and 15 min in the presence of CuZnO@GO nanocomposites under visible light irradiation. Then, 2 mL of 1 mg·mL⁻¹ NBT solution was added to the above solutions and cultured for 30 min at 37 °C. The reaction was stopped by the addition of 0.2 mL of 0.1 mol·L⁻¹ HCl. Then, the reacted suspensions were centrifuged for 10 min at 5000 rpm to remove the supernatants. After that, the collected cells were treated with 1 mL of dimethyl sulfoxide to extract the reduced NBT. Finally, the extracted solution was diluted and the absorbance of the bluish violet formazan obtained from cells was measured at 575 nm by a spectrophotometer.

2.4 Application of CuZnO@GO nanocomposites in circulating cooling water

To assess the photocatalytic antibacterial performance of CuZnO@GO nanocomposites in real samples, the experiments performed in circulating cooling water by using antibacterial rate as an index. The circulating cooling water was taken from petrochemical enterprises and its water quality analysis is shown in Table 1. The amount of viable bacterial cells in the LB agar plates was analyzed using the colony forming units counting [37]. The antibacterial rate was calculated by Eq. (1) as follows:

$$\eta = \frac{n_0 - n}{n_0} \times 100\% \quad (1)$$

where η is antibacterial rate, %; n_0 and n are the numbers of viable bacterial cells in the absence and presence of CuZnO@GO nanocomposites, cfu·mL⁻¹, respectively.

When studying the photocatalytic antibacterial properties of CuZnO@GO nanocomposites in circulating cooling water, the effects of GO mass fraction, dosage of CuZnO@GO and repeated utilization times on antibacterial rate were mainly investigated. The mass fraction of GO was 2.5, 7.5, 12.5, 17.5, 22.5, 27.5, 32.5, 37.5, and 42.5% accounting for CuZnO@GO nanocomposites. The dosage of prepared CuZnO@GO nanocomposites added to the circulating cooling water was 50, 75, 100, 125, and 150 mg·L⁻¹, respectively. After 60 min of exposure to visible light, the antibacterial rate of CuZnO@GO nanocomposites in circulating cooling water was calculated by the colony counting method. For recycling use experiments, the separated CuZnO@GO nanocomposites were washed with distilled water and reused directly for the next antibacterial cycle.

Table 1 Water quality analysis results for circulating cooling water used in the experiment

Index	COD (mg·L ⁻¹)	NH ₄ ⁺ -N(mg·L ⁻¹)	TP (mg·L ⁻¹)	Na ⁺ (mg·L ⁻¹)	Ca ²⁺ (mg·L ⁻¹)	Mg ²⁺ (mg·L ⁻¹)	Turbidity (NTU)	pH
Concentration	182.30	11.75	2.01	289.46	235.21	35.79	5.89	7.56

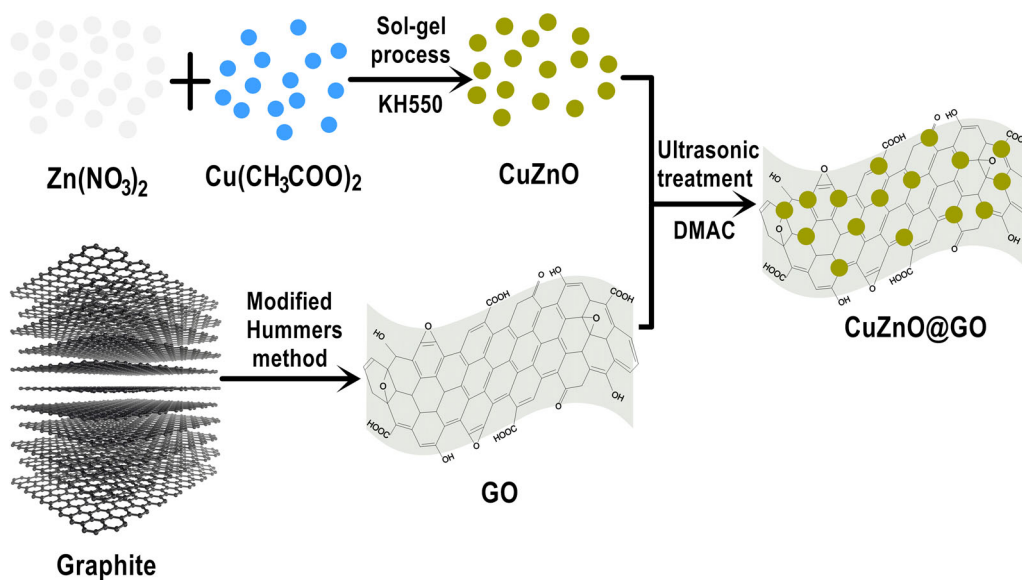


Fig. 1 Synthesis of CuZnO@GO nanocomposites

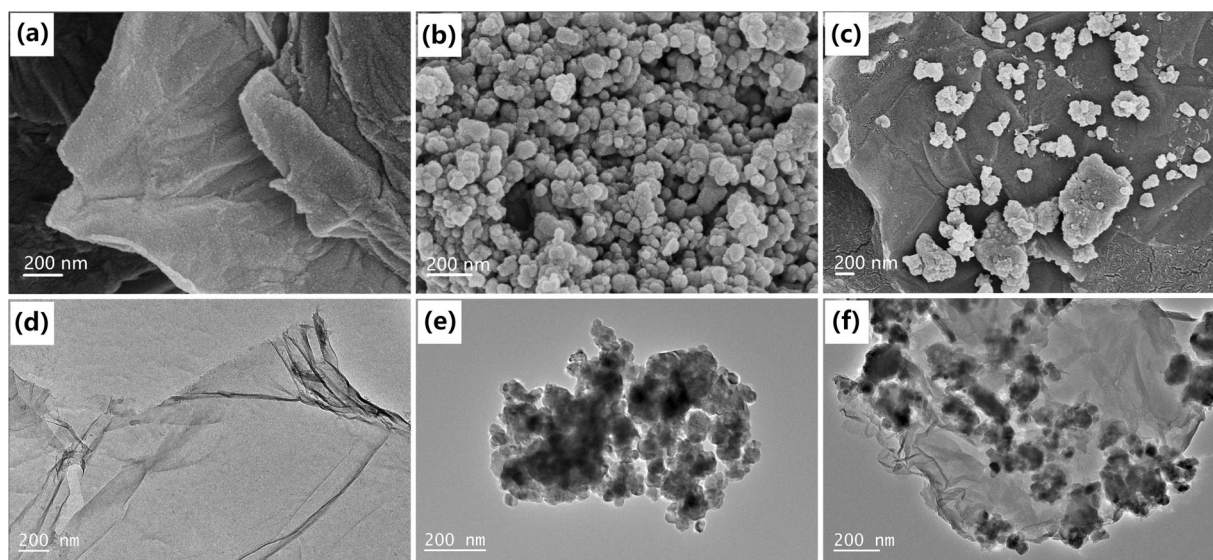


Fig. 2 SEM images of **a** GO, **b** CuZnO, and **c** CuZnO@GO nanocomposites; TEM images of **d** GO, **e** CuZnO, and **f** CuZnO@GO nanocomposites

3 Results and discussion

3.1 Characterization of CuZnO@GO nanocomposites

Figure 1 displays the synthesis procedure of CuZnO@GO nanocomposites. The morphologies and size of GO, CuZnO, and CuZnO@GO samples are observed by SEM and TEM. The SEM and TEM images of GO are displayed in Fig. 2a, d, respectively. It can be clearly seen that GO exhibits a typical two-dimensional sheet structure with characterized wrinkles and high transparency. The SEM

image of CuZnO NPs is shown in Fig. 2b, which reveals the spherical morphology with an average diameter of 20–40 nm. While aggregation of CuZnO NPs is observed from TEM image of CuZnO NPs in Fig. 2e. As presented in Fig. 2c, f, CuZnO NPs have been successfully loaded on GO surface. The large surface area of GO is favorable for the dispersal of CuZnO NPs, which benefits the enhancement of photocatalytic performance.

XRD measurements are employed to determine the phases of the as-prepared materials, and the results are shown in Fig. 3. As can be seen, GO exhibits a high

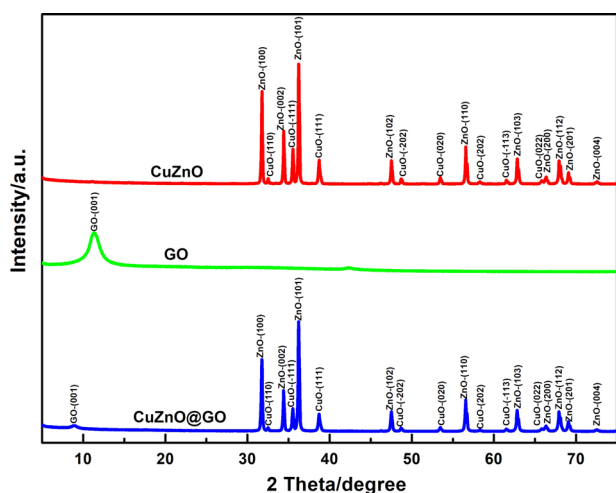


Fig. 3 XRD patterns of GO, CuZnO and CuZnO@GO nanocomposites

intensity diffraction peak centered at 2θ of 11.3° , corresponding to the (001) crystal plane of GO, which is similar to the previous report [38]. In the pattern of CuZnO NPs, strong peaks at scattering angles of 31.7° , 34.3° , 36.2° , 47.5° , 56.5° , 62.8° , 66.4° , 67.9° , 69.1° , and 72.6° are distinctly indexed to the (100), (002), (101), (102), (110), (103), (200), (112), (201), and (004) crystal planes of ZnO (JCPDS No. 80-0074), respectively, indicating the presence of ZnO with hexagonal wurtzite structure in the CuZnO NPs. The intensity and sharpness of diffraction peaks prove that the sample has good crystallinity. In addition, there are some relatively weak diffraction peaks at 2θ of 32.5° , 35.5° , 38.7° , 48.8° , 53.5° , 58.3° , 61.5° and 65.8° in the pattern of CuZnO NPs, which are corresponding to the (110), (-111), (111), (-202), (020), (202), (-113), and (022) crystal planes of CuO (JCPDS No. 89-5895), respectively. The diffraction peaks of CuZnO NPs slightly shift to high angles compared with the pure ZnO standard card, demonstrating that Cu^{2+} has entered the ZnO lattice during the synthesis. Furthermore, CuZnO@GO nanocomposites retain the characteristic diffraction peaks of CuZnO NPs and no other impurity peaks are found, indicating that the morphology of CuZnO NPs has not been changed during the synthesis and CuZnO NPs in the CuZnO@RGO nanocomposites maintain high crystallinity. Besides, a weak GO diffraction peak appears in the composites, which is due to the low amount of GO used in the synthesis process and the unordered accumulation of GO sheets, resulting in low intensity of GO diffraction peak.

The structure of GO, CuZnO, and CuZnO@GO nanocomposites is further analyzed by FT-IR spectra (Fig. 4). The broad absorption peaks around 3427 cm^{-1} are attributed to O–H stretching vibration of H_2O in GO and CuZnO@GO nanocomposites, which may be caused by moisture absorption. In addition, the characteristic peaks at

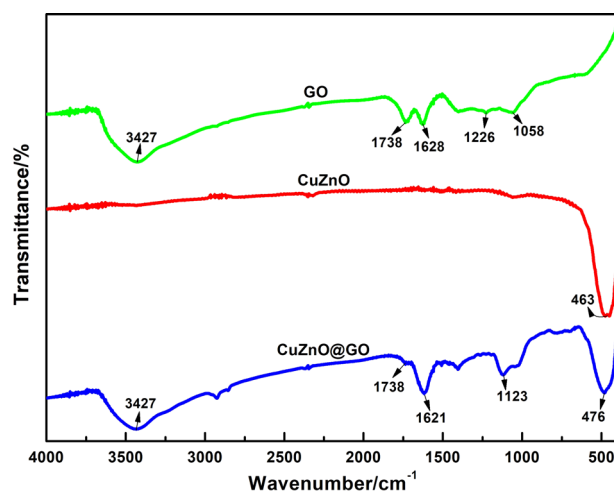


Fig. 4 FT-IR spectra of GO, CuZnO, and CuZnO@GO nanocomposites

1628 cm^{-1} in pure GO and 1621 cm^{-1} in CuZnO@GO nanocomposites are assigned to the C=C stretching band of GO. In the case of GO, the peaks at 1738 , 1226 , and 1058 cm^{-1} are associated with carboxyl C=O, hydroxyl C–O and epoxy C–O groups stretching vibration, respectively. The presence of oxygen-containing functional groups provides active sites for GO, which is conducive to the complex reaction of CuZnO and GO. For CuZnO@GO nanocomposites, there is an obvious absorption peak at 476 cm^{-1} , which is the characteristic absorption peak of CuZnO NPs, and it is proved that CuZnO NPs have been loaded on the surface of GO. Furthermore, an absorption peak at 1123 cm^{-1} appears due to silane coupling agent being used to modify the CuZnO NPs, so that CuZnO@GO nanocomposites show a peak of Si–O stretching vibration.

The optical absorption property of photocatalyst is a key factor which determines its photocatalytic activity. Figure 5a shows the UV–Vis DRS of GO, CuZnO, and CuZnO@GO nanocomposites. GO reveals a certain weak absorption over the entire region, which may be associated with the brownish yellow color of GO. While CuZnO NPs and CuZnO@GO nanocomposites both present strong absorption from UV to visible region and the absorption intensity of CuZnO nanocomposites is higher than that of CuZnO NPs. Compared with CuZnO NPs, CuZnO@GO nanocomposites exhibits red shift of absorption edge toward longer wavelength, which is due to the introduction of GO, resulting the improvement of photocatalytic activity of photocatalyst. To obtain the band gap values, band gap energy plot (Fig. 5b) of materials is deduced by the Tauc plot method [39]. As can be seen, CuZnO NPs and CuZnO@GO nanocomposites provide the band gap energy as 2.87 and 2.64 eV, respectively. These values are lower than the band gap energy of 3.37 eV for pure ZnO, which can effectively reduce the excitation energy of materials, thus

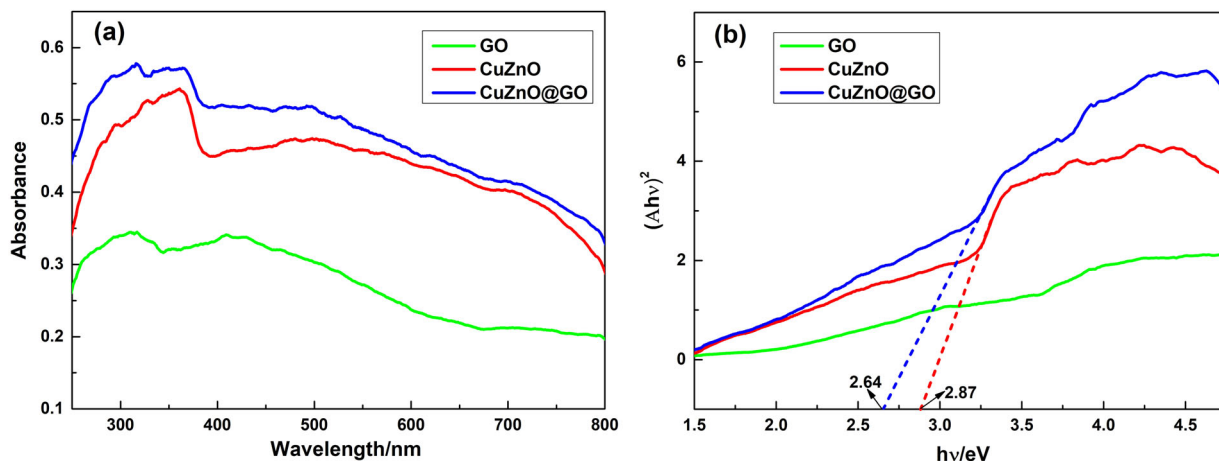


Fig. 5 UV-Vis DRS **a** and band gap energy plot **b** of GO, CuZnO, and CuZnO@GO nanocomposites

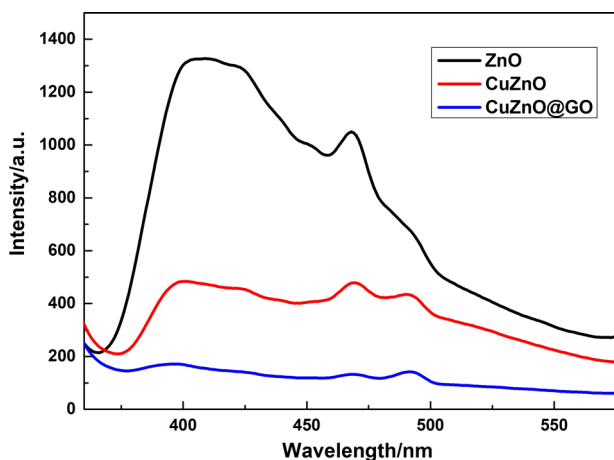


Fig. 6 PL spectra of pure ZnO, CuZnO, and CuZnO@GO nanocomposites with an excitation wavelength of 325 nm

CuZnO@GO nanocomposites have better ability to utilize sunlight.

To further investigate the optical property of samples, PL spectra of photocatalysts are recorded at room temperature and shown in Fig. 6. It can be clearly seen that the spectrum of pure ZnO mainly consists of two emission bands. The first band is the UV near-band-edge emission at 400 nm, which is originated from the recombination of photoinduced electrons and holes [40, 41]. The blue emission at 468 nm is generally occurring due to the oxygen vacancies or other defects of ZnO lattice [42]. By comparison, there is one more emission peak at 490 nm in the spectra of CuZnO NPs and CuZnO nanocomposites than that of pure ZnO, proving more defects existing in photocatalysts, which is beneficial for improving the intensity of visible light emission. In addition, it is observed that the PL intensity of CuZnO NPs decreases dramatically when compared to that of pure ZnO in the entire spectrum. Moreover, CuZnO@GO nanocomposites exhibits the lowest intensity of PL emission

among all three samples, indicating that the recombination rate of photogenerated charge carriers is further reduced. This is because the excited electrons in CuZnO NPs can be efficiently transferred to GO sheets during the photocatalytic process, thereby enhancing the photocatalytic activity of materials. Hence, the incorporation of CuO and GO with ZnO efficiently facilitates the separation of photoinduced electron-hole pairs.

3.2 Antibacterial mechanism of CuZnO@GO nanocomposites against *E. coli* and *S. aureus*

3.2.1 Effect of CuZnO@GO nanocomposites on bacterial protein leakage

From Fig. 7a, we can see that the protein leakage of *E. coli* is very low under normal growth condition, the leakage of 12 h is less than $10 \text{ mg}\cdot\text{L}^{-1}$, and the leakage rate begins to increase after 12 h. There are three reasons for protein leakage in normal bacterial growth. The first is that bacteria discharge some proteins through exocytosis, the second is cell autolysis causes protein leakage, and the third is the normal aging and death of bacteria cause protein leakage. When adding $100 \text{ mg}\cdot\text{L}^{-1}$ CuZnO@GO nanocomposites to *E. coli* suspension, the slope of the curve increases, which proves that the rate of protein leakage is quickened. The main reason is that after the cell membrane of *E. coli* is destroyed by CuZnO@GO nanocomposites, the cell membranes do not prevent substances outflow from cells, which causes the quicker speed of protein leakage, and the protein leakage after 20 h is 10.5 times higher than that in the blank experiment. According to Fig. 7b, the protein leakage of *S. aureus* under normal growth condition is also low, and the leakage of 14 h is less than $10 \text{ mg}\cdot\text{L}^{-1}$. When $100 \text{ mg}\cdot\text{L}^{-1}$ CuZnO@GO nanocomposites are added to the *S. aureus* suspension, the protein leakage speed is accelerated, and the

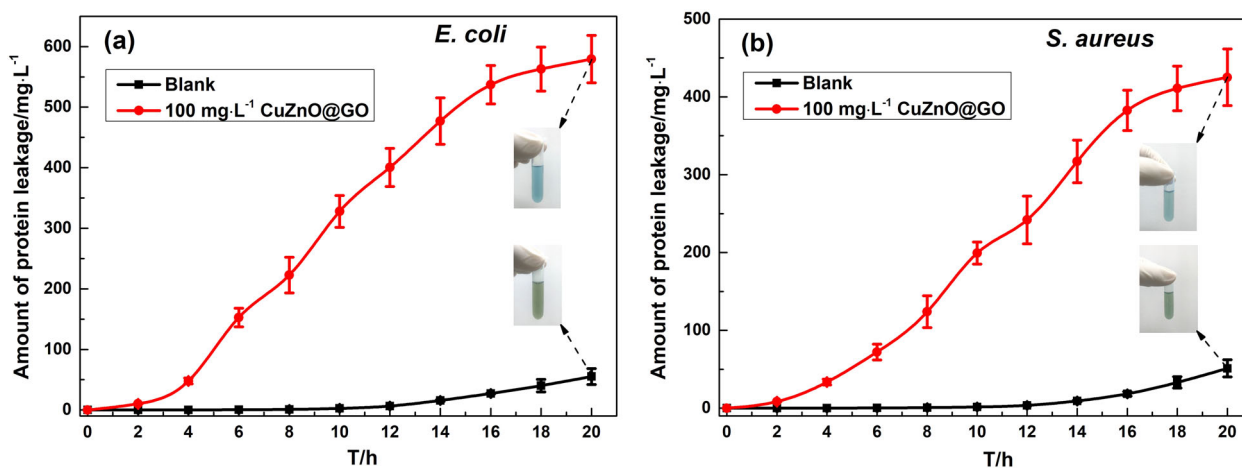


Fig. 7 Effects of CuZnO@GO nanocomposites on protein leakage of **a** *E. coli* and **b** *S. aureus*

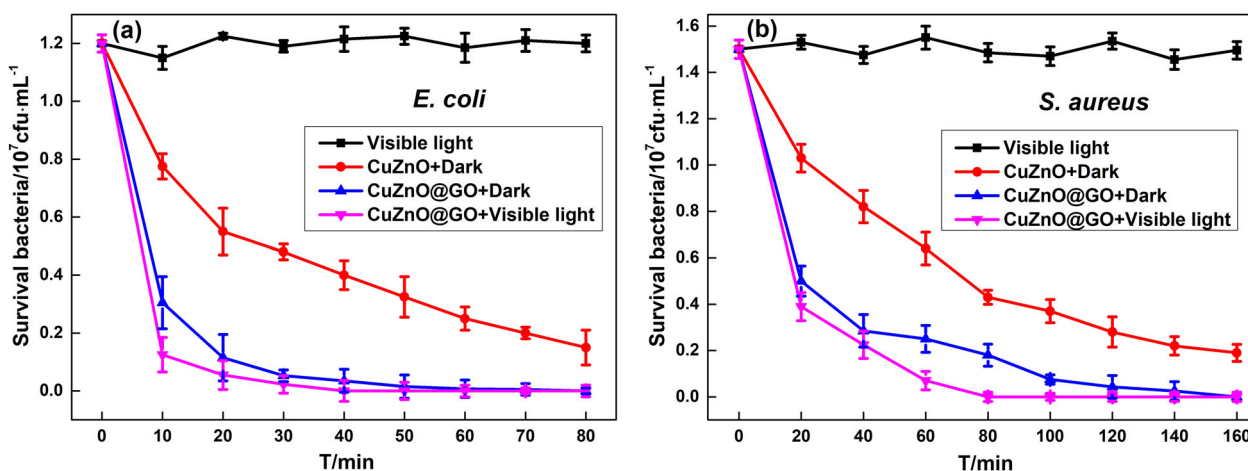


Fig. 8 Antibacterial activity of CuZnO and CuZnO@GO nanocomposites against **a** *E. coli* and **b** *S. aureus*

leakage increases by 8.3 times after 20 h comparing with the blank experiment.

We also can see that after the action of CuZnO@GO nanocomposites, the protein leakage rate of *E. coli* is higher than that of *S. aureus*. This is because that *S. aureus* belongs to gram-positive bacteria. Totally, 90% of the cell wall of gram-positive bacteria is a peptidoglycan with large mechanical strength, and the cell wall is thicker (20–80 nm). Therefore, the cell wall is capable of resisting external injury, and can still maintain the original cell morphology when suffering from external injury. In contrast, *E. coli* belongs to gram-negative bacteria. The cell wall of gram-negative bacteria has a multilayer structure, loose interlayer arrangement, low-peptidoglycan content, and thin cell wall (10–15 nm). Therefore, the ability to resist external injury is weak, and it is easy to cause cell damage and deformation in the case of external injury. Thus the protein leakage rate of *E. coli* is faster than that of *S. aureus*.

3.2.2 Photocatalytic antibacterial activity of CuZnO@GO nanocomposites

In order to evaluate the antibacterial performance of CuZnO@GO nanocomposites, the inactivation experiments for *E. coli* and *S. aureus* were carried out in the presence and absence of visible light and the results are shown in Fig. 8. It is noted that visible light without any materials shows no loss in bacterial cell number for both *E. coli* and *S. aureus*, implying that the visible light itself does not have enough energy to kill bacteria. For dark experiments, the microbes were incubated with CuZnO NPs and CuZnO@GO nanocomposites, respectively. From Fig. 8a, for 100 mg·L⁻¹ CuZnO NPs, the number of survival *E. coli* cells decreases from 1.2 to 0.2 of 10⁷ cfu·mL⁻¹ after treatment for 80 min, which may be attributed to cell permeability change caused by the interaction between the released positively charged zinc and copper ions of CuZnO NPs with the negatively charged cell membrane of bacteria. After loading on GO,

prepared CuZnO@GO nanocomposites possess increased bactericidal efficiency of making all *E. coli* bacteria inactivated after treatment for 80 min in the dark, which proves that GO plays an important role in the antibacterial effect of CuZnO@GO nanocomposites. When visible light is introduced, the antibacterial activity CuZnO@GO

nanocomposites is further enhanced. After 40 min of irradiation time, there are no survival *E. coli* bacteria left, thus CuZnO@GO nanocomposites reveals twice higher antibacterial activity in the presence of visible light than that in the dark. Meanwhile, as can be seen from Fig. 8b, the reduction of viable *S. aureus* bacteria induced by CuZnO@GO nanocomposites displays a similar trend. The difference is that 100% bacterial inactivation time for *S. aureus* treated by CuZnO@GO nanocomposites is 160 min in the dark and 80 min under visible light irradiation, indicating that *S. aureus* is less sensitive to composites than *E. coli*, which is in agreement with previous results.

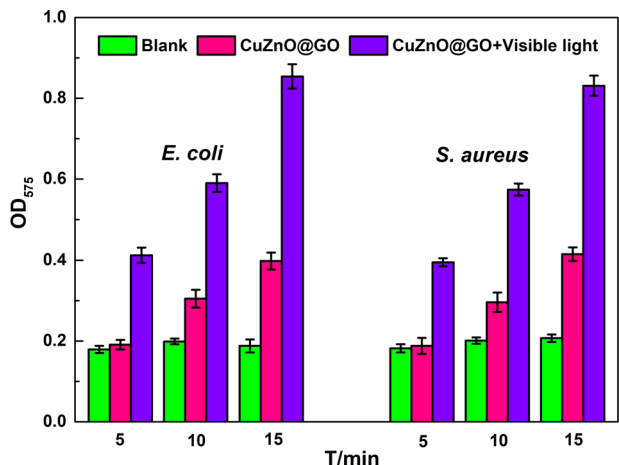
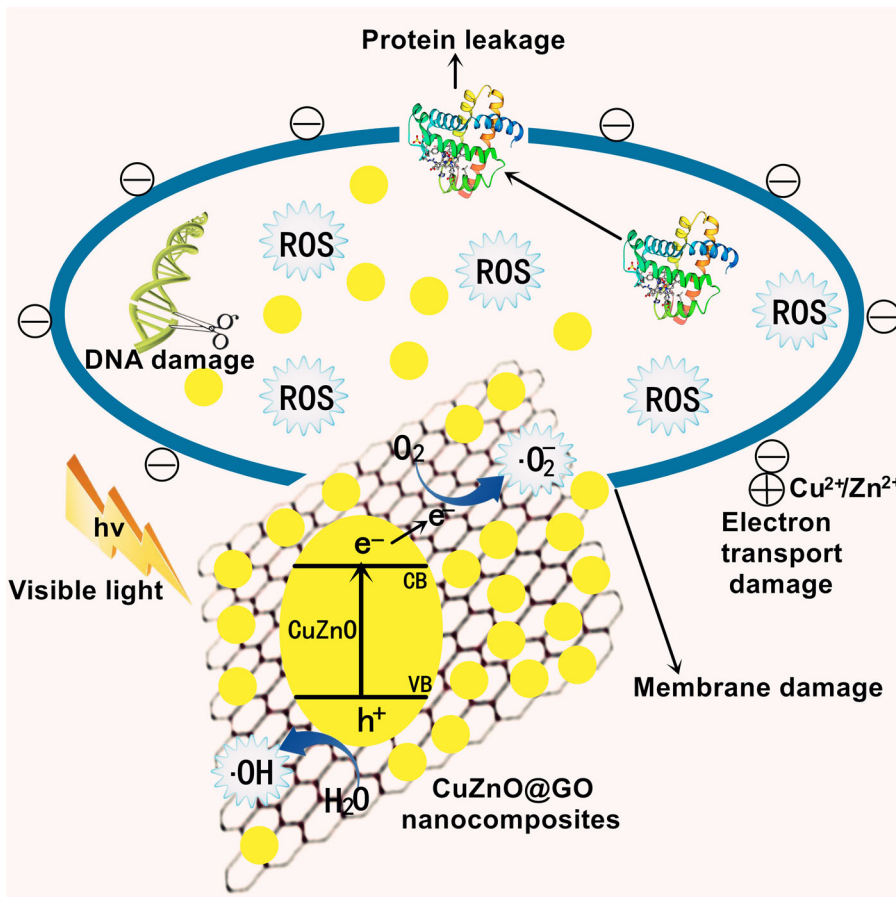


Fig. 9 Effect of CuZnO@GO nanocomposites on the intracellular ROS concentration of *E. coli* and *S. aureus*

3.2.3 Oxidative stress induced by CuZnO@GO nanocomposites

In photocatalytic antibacterial experiments, many researchers reported that ROS acts as a key marker in bactericidal reaction. NBT can be reduced to bluish violet formazan under the action of superoxide radical ($\bullet\text{O}_2^-$), which belongs to a kind of ROS. Therefore, the absorption of formazan can be employed to indicate the level of intracellular ROS in bacteria. As can be seen from Fig. 9, untreated *E. coli* and *S. aureus* cells maintain a stable level of ROS production at

Fig. 10 Schematic of antibacterial mechanism of CuZnO@GO nanocomposites



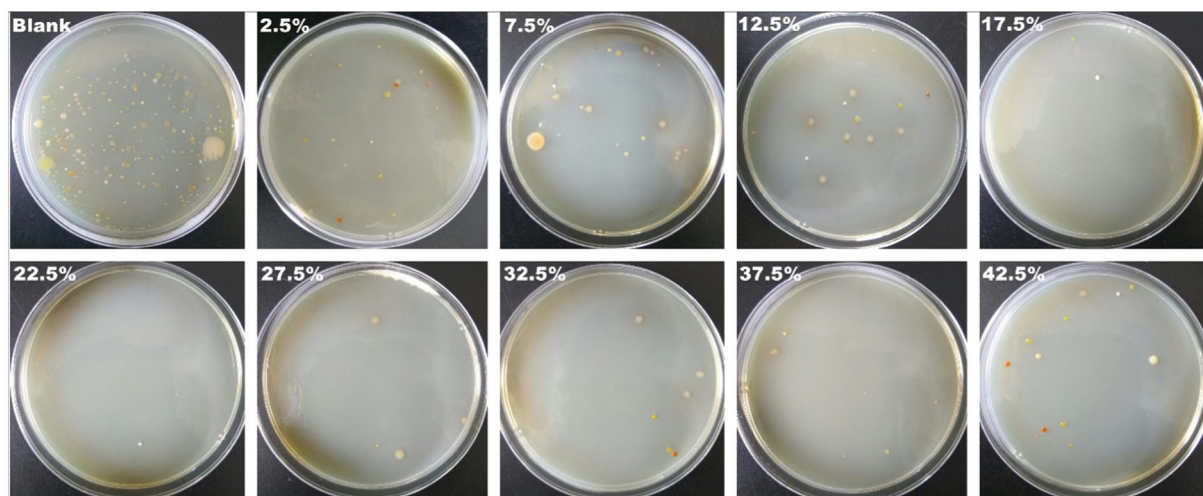


Fig. 11 Antibacterial experiment photos of CuZnO@GO nanocomposites with different GO mass fraction under visible light irradiation

different times. However, after adding CuZnO@GO nanocomposites, the ROS production of *E. coli* and *S. aureus* cells increase with the prolongation of culture time. In 15 min, whether for *E. coli* or *S. aureus*, the intracellular ROS concentration of the bacteria treated by CuZnO@GO nanocomposites is twice higher than that of the blank group. Previous studies have suggested that oxidative stress is one of the mechanisms involved in the antibacterial activity of nanomaterials [43, 44]. When the CuZnO@GO nanocomposites act on *E. coli* or *S. aureus*, the composites itself can induce the electron donor on the cell surface to react with oxygen molecules to generate $\bullet\text{O}_2^-$. More and more reactive oxygen species cannot be removed in time, resulting in the accumulation. Surprisingly, under visible light irradiation, the ROS level of *E. coli* and *S. aureus* cells further increases significantly in the presence of CuZnO@GO nanocomposites and is more than four times higher as compared with those of blank group after 15 min, indicating that illumination plays a vital role in accelerating the rise of intracellular ROS concentration. When the CuZnO@GO nanocomposites are irradiated with visible light, the electrons (e^-) are excited from valence band (VB) to conduction band with the simultaneous creation of holes (h^+) in the VB. Then the generated electrons can be readily trapped by O_2 present on the surface of photocatalyst or bacterial cells to yield $\bullet\text{O}_2^-$. Furthermore, $\bullet\text{O}_2^-$ and the photoinduced holes can react with H_2O in the system to produce strong oxidizing hydroxyl radical ($\bullet\text{OH}$), which can destroy the bacterial cell wall. Additionally, these above ROS can decrease the activity of some membranous enzymes [45] and enter into cells, causing a series of oxidative stress reactions and leading to bacterial death.

Based on the preceding results, the antibacterial mechanism of CuZnO@GO nanocomposites can be proposed and schematically illustrated in Fig. 10. On the one

hand, CuZnO@GO nanocomposites can destroy the cell membrane of bacteria, which leads to the acceleration of cell content leakage. When CuZnO@GO nanocomposites are exposed to bacteria, the nanocomposites can be absorbed onto cells based on the electrostatic interaction between the released positively charged zinc and copper ions of CuZnO NPs with the negatively charged cell membrane of bacteria. Then the electron transport breaks the potential balance on the cell surface and GO can physically cut bacteria due to its sharp edge, resulting the damage of cell structure. On the other hand, CuZnO@GO nanocomposites can induce more oxidative stress in the bacterial cell under visible light irradiation. The illumination leads to the production of electron–hole pairs in photocatalysts and the increased level of ROS in bacteria. These photogenerated radicals with strong oxidation can attack the bacterial cell, causing a series of chemical reaction and leading to bacterial death.

3.3 Antibacterial properties of CuZnO@GO nanocomposites in circulating cooling water

The 0.1 g of modified CuZnO NPs were compounded with GO to make GO mass fraction of 0, 2.5, 7.5, 12.5, 17.5, 22.5, 27.5, 32.5, 37.5, 42.5, and 100%. Then $100 \text{ mg}\cdot\text{L}^{-1}$ CuZnO@GO nanocomposites were added into the circulating cooling water. After stirring for 60 min under visible light irradiation, the antibacterial rate was calculated by Eq. (1). The effect of GO mass fraction on the antibacterial property of CuZnO@GO nanocomposites is expressed by Figs. 11 and 12a.

As can be seen from Fig. 11, the number of bacteria in circulating cooling water decreases significantly after adding CuZnO@GO nanocomposites for 60 min with visible light. When the mass fraction of GO is 17.5%, almost no bacterial

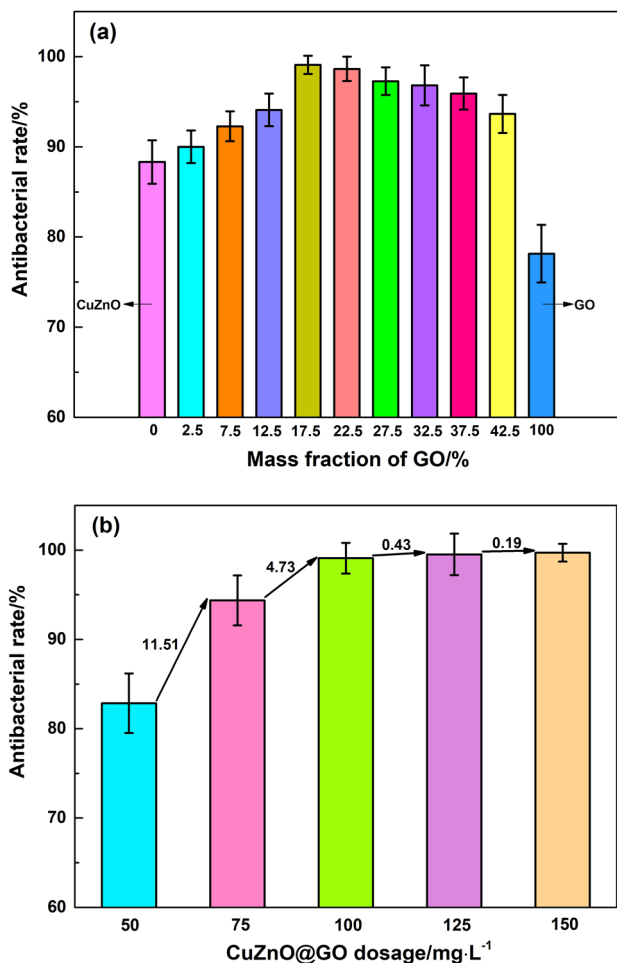


Fig. 12 Effect of **a** GO mass fraction and **b** dosage of composites on antibacterial rate of CuZnO@GO nanocomposites under visible light irradiation

growth is found on the culture dish. According to Fig. 12a, the photocatalytic antibacterial property of CuZnO@GO in circulating cooling water increases with the increase of GO mass fraction, and the highest antibacterial rate reaches 99.09% when the mass fraction of GO is 17.5%. After that, the antibacterial rate of CuZnO@GO decreases with increasing GO mass fraction. CuZnO@GO has positive charge while most of the bacterial surface carries negative charge. When CuZnO NPs are supported on the surface of GO, CuZnO@GO nanocomposites can be well adsorbed on the surface of bacteria by electrostatic action, so that the bacteria will be coated to cut off the exchange of substances and information between bacteria and outside. Besides, the photogenerated electrons excited from CuZnO NPs tends to transfer into GO sheets [46], which can improve the photocatalytic activity. At the same time, the contact chance between bacteria and GO can be increased, and the synergistic effect of CuZnO and GO on antibacterial properties significantly increases the antibacterial rate [47, 48]. When GO mass fraction is higher than 17.5%, the antibacterial rate of the

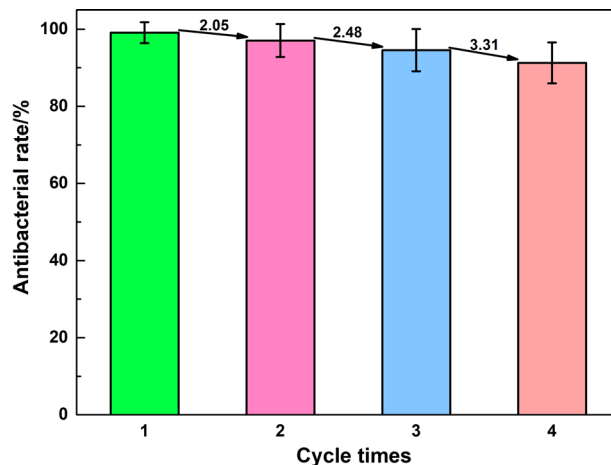


Fig. 13 Reusability of CuZnO@GO nanocomposites in circulating cooling water under visible light irradiation

composites gradually decreases. This is because CuZnO content is not enough to completely fill GO surface when the GO content increases. At the same time, too much GO is agglomerated during the loading process [49], which is detrimental to photocatalysis. After the addition of CuZnO@GO nanocomposites to circulating cooling water, the agglomerated GO instead becomes a substrate for bacterial growth, thereby reducing the antibacterial rate of CuZnO@GO nanocomposites.

The 0.1 g of modified CuZnO NPs were compounded with GO, and the mass fraction of GO was 17.5% of CuZnO@GO nanocomposites. Then CuZnO@GO was added to the circulating cooling water with visible light condition. The effect of CuZnO@GO dosage on the antibacterial rate is shown in Fig. 12b. The antibacterial rate of CuZnO@GO nanocomposites in the circulating cooling water increases with the increase of the dosage. When the dosage is 50 mg·L⁻¹, the antibacterial rate is only 82.85%. When the dosage of CuZnO@GO nanocomposites is increased, the strong antibacterial effect of GO and CuZnO is brought into full play, so that the overall antibacterial property of the composites is significantly enhanced. When the composites dosage is 100 mg·L⁻¹, the antibacterial rate reaches 99.09%. Subsequently, increasing the dosage to 150 mg·L⁻¹, the antibacterial rate steadily increases to 99.71%.

In our previous study, the strains of bacteria were identified in circulating cooling water [50]. The results of the identification showed that there were both gram-negative bacteria (*Enterobacter*, *Proteus*, *Neisseria*, *Pseudomonas*, *Klebsiella*, etc.) and gram-positive bacteria (*Staphylococcus*, *Microbacterium*, etc.) in circulating cooling water. In the complex environment of circulating cooling water, CuZnO@GO nanocomposites can achieve 99.7% of antibacterial rate, which proves the universality of CuZnO@GO nanocomposites.

In order to evaluate the stability and reusability of photocatalyst for realistic application, the recycled runs for the photocatalytic inactivation of bacteria have been performed in circulating cooling water with $100 \text{ mg}\cdot\text{L}^{-1}$ CuZnO@GO nanocomposites for four times (60 min at a time). From Fig. 13, it can be clearly found that the antibacterial rate of CuZnO@GO nanocomposites displays a slight decrease under visible light irradiation after four repeated experiments. The slight reduction of photocatalytic antibacterial activity in cyclic use may be caused by the loss of CuZnO@GO nanocomposites during the centrifugation and washing progress. Moreover, an antibacterial rate of more than 90% is still achieved within 60 min after four runs, demonstrating that CuZnO@GO nanocomposites have considerable photostability. The reusability of CuZnO@GO nanocomposites can save the cost distinctly, thereby facilitating the practical application for water treatment.

4 Conclusions

(1) The size of CuZnO NPs prepared by a sol–gel method was about 20–40 nm. The FT-IR characterization proved that the synthesized GO contained many oxygen-containing functional groups. Through SEM and TEM photos, CuZnO NPs were successfully loaded to the GO surface, and the XRD characterization showed that the lattice morphology of CuZnO NPs did not change after the load. The UV–Vis and PL spectra showed CuZnO@GO nanocomposites had better ability to utilize sunlight.

(2) *E. coli* and *S. aureus* were very sensitive to CuZnO@GO nanocomposites, and CuZnO@GO could accelerate protein leakage of bacteria. When adding CuZnO@GO nanocomposites to *E. coli* or *S. aureus* suspension, the protein leakage after 20 h was 10.5 times or 8.3 times higher than that in the blank experiment. Under visible light irradiation, CuZnO@GO nanocomposites exhibited strong photocatalytic antibacterial activity due to increased oxidative stress in bacterial cell by photo-generated reactive radicals.

(3) In the presence of visible light, the antibacterial rate of CuZnO@GO nanocomposites in circulating cooling water reached 99.09% when the mass fraction of GO was 17.5% and the dosage was $100 \text{ mg}\cdot\text{L}^{-1}$, and more than 90% of bacteria could still be inactivated in 60 min after four recycled runs. The CuZnO@GO nanocomposites could be an efficient visible light-responsive photocatalytic antibacterial agent for the potential application in water treatment.

Acknowledgments This research was financially supported by Natural Science Foundation of Shandong Province, China (ZR201702140013).

Compliance with ethical standards

Conflict of interest The authors declare that they have no conflict of interest.

References

1. Wang HB, Hu C, Hu XX et al. (2012) Effects of disinfectant and biofilm on the corrosion of cast iron pipes in a reclaimed water distribution system. *Water Res* 46(4):1070–1078
2. Batterman S, Eisenberg J, Hardin R et al. (2009) Sustainable control of water-related infectious diseases: a review and proposal for interdisciplinary health-based systems research. *Environ Health Perspect* 117(7):1023–1032
3. Zhang Y, Zhu Y, Yu J et al. (2013) Enhanced photocatalytic water disinfection properties of Bi₂MoO₆-RGO nanocomposites under visible light irradiation. *Nanoscale* 5(14):6307–6310
4. Krasner SW, Weinberg HS, Richardson SD et al. (2006) Occurrence of a new generation of disinfection byproducts. *Environ Sci Technol* 40(23):7175–7185
5. Jafry HR, Liga MV, Li QL et al. (2011) Simple route to enhanced photocatalytic activity of P25 titanium dioxide nanoparticles by silica addition. *Environ Sci Technol* 45(4):1563–1568
6. Chong MN, Jin B, Chow CWK et al. (2010) Recent developments in photocatalytic water treatment technology: a review. *Water Res* 44(10):2997–3027
7. Kasinathan K, Kennedy J, Elayaperumal M et al. (2016) Photodegradation of organic pollutants RhB dye using UV simulated sunlight on ceria based TiO₂ nanomaterials for antibacterial applications. *Sci Rep* 6:1–12
8. Kumar R, Anandan S, Hembram K et al. (2014) Efficient ZnO-based visible-light-driven photocatalyst for antibacterial applications. *ACS Appl Mater Interfaces* 6(15):13138–13148
9. Liu C, Kong D, Hsu PC et al. (2016) Rapid water disinfection using vertically aligned MoS₂ nanofilms and visible light. *Nat Nanotech* 11(12):1098–1104
10. Luo M, Liu Y, Hu JC et al. (2012) One-pot synthesis of cds and ni-doped cds hollow spheres with enhanced photocatalytic activity and durability. *ACS Appl Mater Interfaces* 4(3):1813–1821
11. Piccirillo C, Pinto RA, Tobaldi DM et al. (2015) Light induced antibacterial activity and photocatalytic properties of Ag/Ag₃PO₄-based material of marine origin. *J Photochem Photobiol* 296:40–47
12. Kumar S, Dhiman A, Sudhagar P et al. (2018) ZnO–graphene quantum dots heterojunctions for natural sunlight-driven photocatalytic environmental remediation. *Appl Surf Sci* 447:802–815
13. Choina J, Bagabas A, Fischer C et al. (2015) The influence of the textural properties of ZnO nanoparticles on adsorption and photocatalytic remediation of water from pharmaceuticals. *Catal Today* 241:47–54
14. Kavitha T, Gopalan AI, Lee KP et al. (2012) Glucose sensing, photocatalytic and antibacterial properties of graphene–ZnO nanoparticle hybrids. *Carbon N Y* 50(8):2994–3000
15. Sakthivel S, Neppolian B, Shankar MV et al. (2003) Solar photocatalytic degradation of azo dye: comparison of photocatalytic efficiency of ZnO and TiO₂. *Sol Energy Mat Sol C* 77(1):65–82
16. Sirelkhatim A, Mahmud S, Seeni A et al. (2015) Review on zinc oxide nanoparticles: antibacterial activity and toxicity mechanism. *Nano Micro Lett* 7(3):219–242
17. Ghosh S, Goudar VS, Padmalekha KG et al. (2012) ZnO/Ag nanohybrid: synthesis, characterization, synergistic antibacterial activity and its mechanism. *Rsc Adv* 2(3):930–940

18. Yousefi R, Jamali SF, Cheraghizade M et al. (2016) Synthesis and characterization of Pb-doped ZnO nanoparticles and their photocatalytic applications. *Mater Res Innov* 20(2):121–127
19. Yu C, Yang K, Xie Y et al. (2013) Novel hollow Pt–ZnO nanocomposite microspheres with hierarchical structure and enhanced photocatalytic activity and stability. *Nanoscale* 5(5):2142–2151
20. Fakhri A, Azad M, Tahami S (2017) Degradation of toxin via ultraviolet and sunlight photocatalysis using ZnO quantum dots/CuO nanosheets composites: preparation and characterization studies. *J Mater Sci Mater Electron* 28(21):1–6
21. Wu W, Zhang S, Xiao X et al. (2012) Controllable synthesis, magnetic properties, and enhanced photocatalytic activity of spindle-like mesoporous α -Fe₂O₃/ZnO core-shell heterostructures. *ACS Appl Mater Interfaces* 4(7):3602–3609
22. Subhan MA, Uddin N, Sarker P (2015) Photoluminescence, photocatalytic and antibacterial activities of CeO₂-CuO-ZnO nanocomposite fabricated by co-precipitation method. *Spectrochim Acta A Mol Biomol Spectrosc* 149(46):839–850
23. Liu J, Li F, Liu C et al. (2014) Effect of Cu content on the antibacterial activity of titanium–copper sintered alloys. *Mater Sci Eng* 35(1):392–400
24. Baek YW, An YJ (2011) Microbial toxicity of metal oxide nanoparticles (CuO, NiO, ZnO, and Sb₂O₃) to *Escherichia coli*, *Bacillus subtilis*, and *Streptococcus aureus*. *Sci Total Environ* 409(8):1603–1608
25. Zhao J, Wang Z, Dai Y et al. (2013) Mitigation of CuO nanoparticle-induced bacterial membrane damage by dissolved organic matter. *Water Res* 47(12):4169–4178
26. Cruz G, Gómez MM, Solís JL et al. (2018) Composites of ZnO nanoparticles and biomass based activated carbon: adsorption, photocatalytic and antibacterial capacities. *Water Sci Technol* 2017(2):492–508
27. Akhavan O, Azimirad R, Safa S (2011) Functionalized carbon nanotubes in ZnO thin films for photoinactivation of bacteria. *Mater Chem Phys* 130(1):598–602
28. Papageorgiou DG, Kinloch LA, Young RJ (2017) Mechanical properties of graphene and graphene-based nanocomposites. *Prog Mater Sci* 90:75–127
29. Pumera M (2013) Electrochemistry of graphene, graphene oxide and other graphenoids: review. *Electrochem Commun* 36(6):14–18
30. De JN, Allieux M, Oostveen JT et al. (2005) Optical performance of carbon-nanotube electron sources. *Phys Rev Lett* 94(18):1–4
31. Ueki Y, Aoki T, Ueda K et al. (2017) Thermophysical properties of carbon-based material nanofluid. *Int J Heat Mass Transf* 113:1130–1134
32. Hu W, Peng C, Luo W et al. (2010) Graphene-based antibacterial paper. *ACS Nano* 4(7):4317–4323
33. Akhavan O, Ghaderi E (2010) Toxicity of graphene and graphene oxide nanowalls against bacteria. *ACS Nano* 4(10):5731–5736
34. Lian P, Zhu X, Liang S et al. (2010) Large reversible capacity of high quality graphene sheets as an anode material for lithium-ion batteries. *Electrochim Acta* 55(12):3909–3914
35. He M, Wu T, Pan S et al. (2014) Antimicrobial mechanism of flavonoids against *Escherichia coli*, ATCC 25922 by model membrane study. *Appl Surf Sci* 305:515–521
36. Banerjee M, Mallick S, Paul A et al. (2010) Heightened reactive oxygen species generation in the antimicrobial activity of a three component iodinated chitosan-silver nanoparticle composite. *Langmuir* 26(8):5901–5908
37. Novakowski KE, Loukov D, Chawla V et al. (2017) Bacterial binding, phagocytosis, and killing: measurements using colony forming units. *Methods Mol Biol* 1519:297–309
38. Zhang CC, Chen MX, Xu XY et al. (2014) Graphene oxide reduced and modified by environmentally friendly glycyglycine and its excellent catalytic performance. *Nanotechnology* 25(13):1–12
39. Yan B, Yue G, Yang J et al. (2013) On the bandgap of hydrogenated nanocrystalline silicon intrinsic materials used in thin film silicon solar cells. *Sol Energy Mat Sol C* 111(1):90–96
40. Lim J, Shin K, Kim HW et al. (2004) Effect of annealing on the photoluminescence characteristics of ZnO thin films grown on the sapphire substrate by atomic layer epitaxy. *Mater Sci Eng* 107(3):301–304
41. Yang J, Zheng J, Zhai H et al. (2010) Oriented growth of ZnO nanostructures on different substrates via hydrothermal method. *J Alloy Compd* 489(1):51–55
42. Zhang Y, Mu J et al. (2007) Controllable synthesis of flower- and rod-like ZnO nanostructures by simply tuning the ratio of sodium hydroxide to zinc acetate. *Nanotechnology* 18(7):1–6
43. Liu S, Zeng TH, Hofmann M et al. (2011) Antibacterial activity of graphite, graphite oxide, graphene oxide, and reduced graphene oxide: membrane and oxidative stress. *ACS Nano* 5(9):6971–6980
44. Wahab R, Siddiqui MA, Saquib Q et al. (2014) ZnO nanoparticles induced oxidative stress and apoptosis in HepG2 and MCF-7 cancer cells and their antibacterial activity. *Colloid Surf B* 117(7):267–276
45. Padmavathy N, Vijayaraghavan R (2011) Interaction of ZnO nanoparticles with microbes—a physio and biochemical assay. *J Biomed Nanotechnol* 7(6):813–822
46. Lv XJ, Fu WF, Chang HX et al. (2012) Hydrogen evolution from water using semiconductor nanoparticle/graphene composite photocatalysts without noble metals. *J Mater Chem* 22(4):1539–1546
47. Zhang L, Ding Y, Povey M et al. (2008) ZnO nanofluids—a potential antibacterial agent. *Prog Nat Sci Mater* 18(8):939–944
48. Liu S, Hu M, Zeng TH et al. (2012) Lateral dimension-dependent antibacterial activity of graphene oxide sheets. *Langmuir* 28(33):12364–12372
49. Some S, Ho SM, Dua P et al. (2012) Dual functions of highly potent graphene derivative poly-L-lysine composites to inhibit bacteria and support human cells. *ACS Nano* 6(8):7151–7161
50. Liu F, Zhao CC, Xia L et al. (2011) Biofouling characteristics and identification of preponderant bacteria at different nutrient levels in batch tests of a recirculating cooling water system. *Environ Technol* 32(8):901–910